Electromagnetic – thermal coupled optimization of high power traction drive induction machines

M. A. Vogelsberger, J. Buschbeck*, A. Orellano*
Bombardier Transportation Austria GmbH
Hermann-Gebauer-Straße 5, 1220 Vienna, Austria
*Bombardier Transportation GmbH
Am Rathenaupark, 16761 Hennigsdorf, Germany

E. Schmidt, M. Bazant**
Vienna University of Technology, Inst. of. Energy Systems and Elect. Drives, Gußhausstrasse 25, 1040 Vienna, Austria
**Bombardier Transportation (Switzerland) Ltd.
Brown Boveri-Strasse 5, 8050 Zurich, Switzerland

Abstract **– In the electrical machines, operated in railway traction drives, the growth of power density requires overproportional more heat to be discharged which leads to the need for more and more advanced cooling techniques. A novel optimization and evaluation approach for internal air cooled traction machines will be presented in this paper. It analyses and investigates the thermo-aero- and thermodynamic cooling performance combined with the electromagnetic performance. As a first step, analytical models are used to speed up calculation time for obtaining pressure drop, volume flow distribution and heat transfer as well as iron stack temperature. The results are validated using CFD (computational fluid dynamics simulations) of several iron stack cooling duct geometries. Finally, an approach is presented about on the optimization can be implemented, by coupling the analytic thermal model, CFD tool and electromagnetic losses obtained by finite element analysis.**

***Keywords*— analytical models, AC motor drives, design optimization, induction machines, thermal management of electronics, traction motors**

I. INTRODUCTION

Based on the lack of space envelope in railway traction drive applications (e.g. limited by track gauge) and the request of increased power for traction drives in locomotives, trams, and metros asynchronous induction machines used in traction drives always show much higher electromagnetic and thermal utilization in comparison to standard industrial variable speed drives. Thermal restrictions (e.g. of insulation material, bearings) as well as other conditions defined from the application (e.g. water/air cooling; forced/self-ventilation, converter inputs, tractive force curve) which strongly influences the design of such machines.

Consequently, an optimization with respect to a maximum electromagnetic performance and the thermal limitations must consider fundamental aspects of electromagnetic, thermal and mechanical loadabilities. Additionally, the characteristics of these machines, in particular torque density and stray field inductances, have to be taken into account with the multi-domain optimization.

This work was supported by Bombardier Transportation:
Product Development PPC-Drives/GSC (PDev), CoC Aero- & Thermo-dynamics, and REA Region Central and Eastern Europe and CIS.

II. LOADABILITY ASPECTS

The ratio of stacking length l_i and pole pitch τ_p of induction machines depends on the number of pole pairs p and lies within a typical range of

$$\chi = \frac{l_i}{\tau_p} = (1 \dots 2)\sqrt[3]{p}\,. \tag{1}$$

Therefore, typical lengths of induction machines can be assumed to be variable over a length scale λ such as stacking length l_i and air-gap diameter D_i [1].

A. Mechanical Loadability

As stated in [1], the maximum speed of an induction machine becomes inversely proportional to the scale,

$$n_{max} \sim \frac{1}{\lambda}. \tag{2}$$

This also holds for the maximum supply frequency, since synchronous rotor speed and stator frequency are proportional.

B. Thermal Loadability

In general, the stationary temperature rise ΔT of an electrical machine caused by any losses P_L follows from

$$\Delta T \sim \frac{P_L}{A_T}\,, \quad A_T \sim \lambda^2\,, \tag{3}$$

where the cooling surface A_T depends quadratically on the scale.

C. Electric Loadability

The power losses of any winding can be written as

$$P_{Cu} \sim J^2\,\lambda^3\,. \tag{4}$$

The temperature rise caused by such losses is directly proportional to the product of the RMS value of the current sheet of the armature winding A and the current density J of the winding conductors,

$$\Delta T \sim \frac{P_{Cu}}{A_T} \sim A\,J\,, \tag{5}$$

which is independent of the scale of an electrical machine [2]. Thus, with respect to temperature rise and consequently cooling methods the product $A \cdot J$ is one of the most important design criteria.

D. Magnetic Loadability

Thereby, magnetic flux density B_δ within the air-gap and supply frequency f determine the hysteresis losses $P_{Fe,Hy}$ and eddy current losses $P_{Fe,EC}$ within the laminated iron as given by

$$P_{Fe,Hy} \sim f\,B_\delta^2\,\lambda^3, \quad P_{Fe,EC} \sim f^2\,B_\delta^2\,\lambda^3\,. \tag{6}$$

With the constant field region, the hysteresis losses are more significant at lower speeds. On the one hand, the eddy current losses will become more interesting with higher speeds. On the other hand, in the field weakening range with $B_\delta\,f \approx$ const, these losses are rather decreasing or constant.

E. Torque density

The well-known Esson utilization number $C_{IM} = \pi^2\,\tau_\delta$ defines the apparent power S_{IM} of the induction machine in dependence on air-gap diameter D_i, stacking length l_i and synchronous speed n_s as given by

$$S_{IM} = C_{IM}\,D_i^2\,l_i\,n_s\,. \tag{7}$$

However, the apparent torque T_{IM} of the induction machine follows from

$$T_{IM} = \frac{S_{IM}}{2\,\pi\,n_s} = 2\,\tau_\delta\,V_\delta\,, \tag{8}$$

and is proportional to the product of tangential stress τ_δ and volume

$$V_\delta = \frac{\pi}{4}\,D_i^2\,l_i \sim \lambda^3\,. \tag{9}$$

The maximum average tangential stress τ_δ within the air-gap of an induction machine is given by

$$\tau_\delta = \frac{1}{\sqrt{2}}\xi_1\,A\,B_\delta\,, \tag{10}$$

where A denotes the RMS value of the armature current sheet, B_δ the magnitude of the fundamental wave of the radial component of the magnetic flux density within the air-gap and ξ_1 is the total winding factor including pitch, distribution and, if applicable, skewing terms.

F. Stray Field Inductances

Typically, the most important portion of the stray field inductances arises from stator and rotor slots. The normalized values of these stray field inductances are proportional to the stray coefficient of the slots λ_σ and can be written as

$$l_\sigma \sim \lambda_\sigma\,\frac{A}{B_\delta}\,. \tag{11}$$

Consequently, these inductances depend on current sheet A and air-gap flux density B_δ. It should be noted, that the stray coefficient λ_σ is proportional to the slot height to width ratio.

In order to achieve a high field weakening capability of the induction machine, the torque characteristic must provide a ratio of maximum torque to nominal load torque as the factor of the desired field weakening range. Therefore, the stray field inductances must not change significantly when starting from an initial design which fulfills the criteria of the application.

G. Summary

By keeping electric as well as magnetic utilization constant, the losses of an induction machine (4) and (6), grow with the third of the length scale. However, the cooling surface grows only to the square of the scale. As a consequence, an increased scale of an electrical machine yields more and more importance for the cooling methods.

Assuming a given temperature rise due to the rather load-independent iron losses, the magnetic flux density can vary in the range of

$$B_\delta \sim \lambda^{0.5} \ldots \lambda\,. \tag{12}$$

As given above, the stray field inductances should be kept constant.

$$A \sim B_\delta \sim \lambda^{0.5} \ldots \lambda\,. \tag{13}$$

Therefore, the maximum average tangential stress depends on the scale as given by

$$\tau_\delta \sim \lambda \ldots \lambda^2 \tag{14}$$

and the maximum torque T_{IM} of an induction machine (8) grows with the scale as of

$$T_{IM} \sim \lambda^4 \ldots \lambda^5\,. \tag{15}$$

However, an increasing armature current sheet A asks for a decreasing current density J within the windings. But the stray field inductances restrict rather to a constant current density. Furthermore, as given by (5), the cooling of the load-dependent losses asks for efficient cooling methods additionally [3,4].

III. Temperature Distribution

Presuming some simplifications like constant temperature in angular direction, then 1D temperature field equation can be solved analytically with given heat source terms to model the temperature distribution within the machine. Assuming heat source per volume $\dot{W}$ and conductivity k to be piecewise constant the temperature field is given with

$$T(r) = -\frac{\dot{W}r^2}{4\,k} + c_a + c_b \ln\frac{r}{r_0}, \qquad (16)$$

where c_a and c_b are constants to be defined by boundary conditions. In the center symmetry condition is applied and between parts no isolation is present, thus no step change in temperature occurs and housing temperature must be given. In Fig. 1 the resulting temperature distribution with temperature differences to housing temperature is shown. The air-gap is modeled as heat conducting only thus heat transfer through convection is assumed not to be present. This results in an overestimated thermal insulation between stator and rotor. However, in the presented case no heat is transferred through the air-gap due to equal sink and source terms in stator and rotor, respectively.

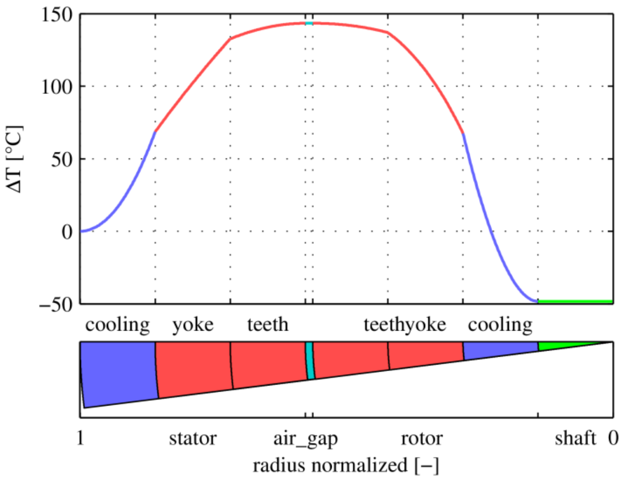

Fig. 1. Temperature distribution 1D model (top), visualization of sink/ source locations in the stacking cross section (bottom).

Due to changing conductances a bend in curve shape occurs on joints between parts. No heat is exchanged through the housing because heat source and sink terms equal out. It results a temperature gradient to the outside of zero.

The model overestimates temperature change due to no heat exchange through the front and back sides. The magnified thermal insulation of the air-gap leads to higher temperature differences between stator and rotor if the corresponding sink and source terms do not equal out. However, from this general observation it can be concluded that a positive net heat flux in the rotor should drastically be avoided.

IV. Optimization Strategy

Different cooling duct configurations are investigated where cooling fluid passes axially through stator and rotor iron stack. Cooling ducts can be placed in whole iron yoke areas, see Fig. 2.

The optimization evaluates both the electromagnetic performance as well as the iron stack temperature required for heat removal. The two evaluations are one way coupled; within the electromagnetic calculation the heat sources for the thermal model are determined

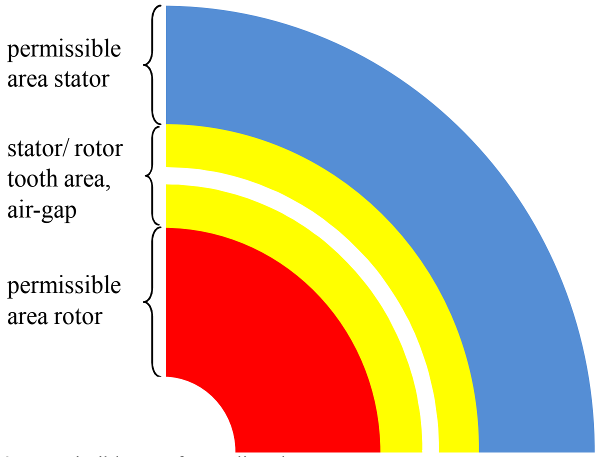

Fig. 2: Permissible area for cooling ducts.

Fig. 3 shows the optimization loop. Each step is described in the following subsections.

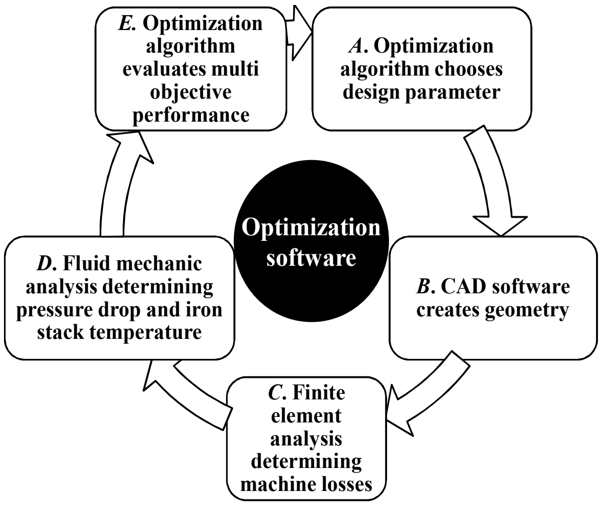

Fig. 3: Optimization loop.

A. Parameters

The parameters are listed in Table 1; Fig. 4 shows the nomenclature used.

Table 1

Parameters conversion with ranges

Parameter	Geometric quantity	Parameter range	Geometric range
f_position_r,s	position_r,s	[0, 1]	[R_min, R_max]
a_r,s		[0.001, 0.2]	
f_b_r,s	b_r,s	[0, 1]	[≈0, b_max]
f_c_r,s	c_r,s	[0, 2]	[0, 2a_r,s]
f_r_a_r,s	r_a_r,s	[0, 1]	[0, r_a_max]
f_r_c_r,s	r_c_r,s	[0, 1]	[0, r_c_max]
f_rotor_stator	no_ducts_r,s	[0, 1]	[2, ∞]
p_soll		[0, 1559.5]	

The indices r and s denote the parameter for rotor and stator, respectively. The prefixed 'f' for function of the parameter name marks the difference to the actual geometric quantity. In total there are 14 parameters describing 14 geometric quantities.

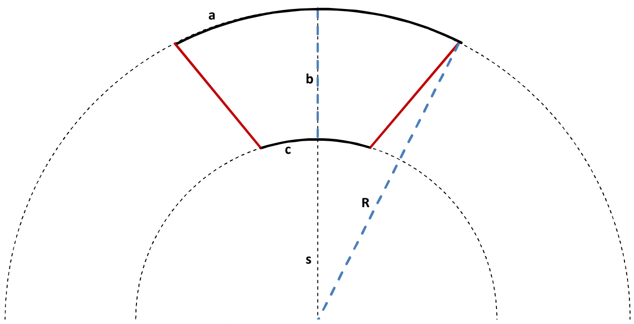

Fig. 4: Parameter nomenclature.

The workflow is structured in three parts: First, the shape of the ducts is constructed converting the parameters to geometric quantities. Next, the area and circumference of the ducts are calculated. Then, the duct numbers can be obtained in such a way to fulfill the pressure and flow distribution constraints. Analytical formulae are used to calculate flow state which is presented in section V.

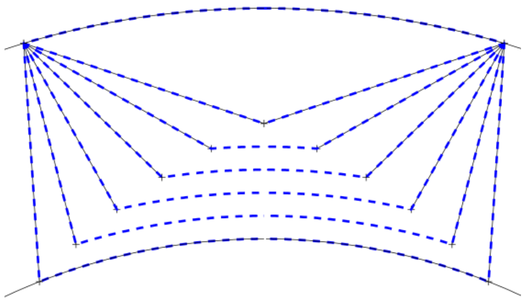

Fig. 5. Variation in duct height and lower edge length in respect to upper edge, respectively.

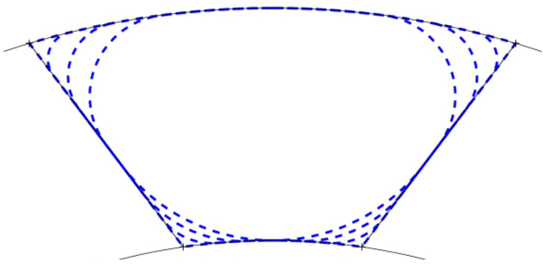

Fig. 6. Variation in upper and lower radius.

B. *Geometry Creation*

The CAD software is able to allocate every design input to a parameter. After geometry creation, a 2D geometry is exported for the finite element analysis whereas the computational fluid dynamics (CFD) needs the full 3D model.

C. *Electromagnetic Evaluation*

The electromagnetic evaluation is automated by a script driven finite element analysis.

Preprocessing: First, the geometry is imported and the predefined mesh settings are applied, physic quantity definitions like material properties, supply voltage sources, etc. are loaded.

Solving: Two cases are calculated. To obtain magnetizing current and average flux densities in tooth and yoke region no load state is simulated. In a second run, the load case defines iron losses as well as resistive losses.

Open source MUMPS[1] is used, a direct solver capable of utilizing parallelization. The advantage here is that the solver can allocate its own memory in addition to reserved memory by the software [5]. Then, solving parameters like precision, iteration number and relaxation factor are defined and the two solving scenarios 'load case' and 'no load case' are set up.

Postprocessing: After performed calculation the needed output values are computed. To consider additional losses e.g. due to the deterioration of the sheet permeability after the stamping process, Bombardier Transportation's internal equations for loss prediction are used to obtain values closer to measurements performed before.

Fig. 7 shows the instationary magnetic flux distribution of an example design created by the optimization software.

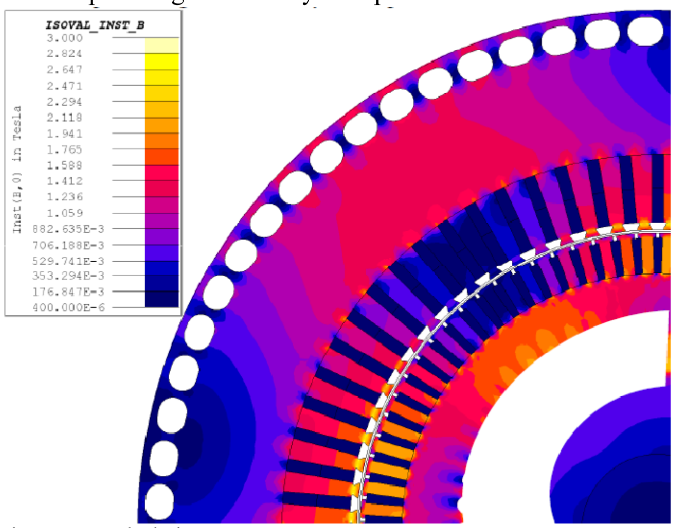

Fig. 7: Example design.

D. *Fluid Mechanical Analysis*

The fluid mechanical analysis is performed analytically. First, the pressure loss is determined using pipe pressure drop coefficients from [6]. Second, the heat transfer coefficient is obtained with an empirical approach to calculate the Nusselt number. Then, the surface temperature is iterated until steady state is reached and discharged energy is equal to the loss heat source terms. The analytical model used is described in part V.

E. *Optimization Algorithm*

Optimization algorithms must choose designs in a way the (pareto) optimum is reached with minimal design evaluations

[1] Stands for Multifrontal Massively Parallel sparse direct Solver, see http://mumps.enseeiht.fr.

required. For this purpose the group of evolutionary algorithms mimic the natural selection process. In this analogy, a single gene is equivalent to a parameter, a chromosome to one design and the design space is equivalent to the whole population.

To create new designs the Multi-Objective Genetic Algorithm (MOGA-II) is used applying the following mechanisms [7]:

- Crossover interchanges sections of the chromosomes of parent designs with a certain probability.
- Mutation modifies a single gene, and the mutation ration defines hereby the percentage of modified genes.
- Selection and elitism ensures the preservation of best designs in the population [8].

V. ANALYTIC MODEL

Analytical formulae are used to cover pressure loss calculation as well as iron stack temperature calculation. All formulae and coefficients used for obtaining pressure loss and heat transfer are given in [6].

The pressure loss of a single duct is calculated

$$\Delta p = \sum \zeta_i \cdot \frac{\rho\, v^2}{2}, \tag{17}$$

with ζ_i being a pressure drop coefficient for tube, inflow and outflow, v is the mean flow velocity and ρ the density. For the tube pressure drop coefficient ζ_{tube} formula from HERMANN (18) is used valid in present Reynolds number range (2300 < Re<2·106

$$\zeta_{tube} = \left(0.00540 + \frac{0.3964}{\mathrm{Re}^{0.3}}\right)\frac{l}{d}, \tag{18}$$

with duct length l and duct diameter d. [6] gives for inflow pressure drop coefficients with sharp edges $\zeta_{inflow} = 0.5$. Caused by the relative movement of the rotor the flow enters the rotor ducts with an angle δ. With (19) the coefficient increase can be approximated to $\zeta_{inflow,rotor} \approx 0.75$.

$$\zeta_{inflow,rotor} = 0.3\cos\delta + 0.2\cos^2\delta \tag{19}$$

On the outlet the flow experiences a drastic change in cross section area A_1/A_2 leading to the pressure drop coefficient

$$\zeta_{outflow} = \left(1 - \frac{A_1}{A_2}\right)^2. \tag{20}$$

In a parallel configuration of ducts the pressure drop before inlet and after outlet must be equal. A script iterates the volume flow distribution and therefore the mean velocities in the tubes in such a way to utilize the same pressure drop. Non circular tubes cross sections are covered using the common *hydraulic diameter* which is derived using the shear stress approach.

The heat transfer is modeled with an empirical formula for the Nusselt number which is describing the ratio between convection and conduction heat transfer.

Equation (24) is valid for flow states with Reynolds numbers between $10^4 \leq \mathrm{Re} \leq 10^6$ and Prandtl numbers in the range of $0.6 \leq \mathrm{Pr} \leq 1000$.

Equation (21) describes heat transfer per surface $\dot{q}$ with logarithmic temperature $\Delta T_{\ln}$ given in (22) where T_W is the wall temperature, T_{in} and T_{out} the in- and outflow temperature, respectively.

$$\dot{q} = \alpha\, \Delta T_{ln} \tag{21}$$

$$\Delta T_{ln} = \frac{(T_W - T_{in}) - (T_W - T_{out})}{\ln\left(\frac{T_W - T_{in}}{T_W - T_{out}}\right)} \tag{22}$$

The heat transfer coefficient α needs to be determined with the Nusselt number given in (24)

$$\alpha = \frac{\mathrm{Nu}\, k}{d}. \tag{23}$$

$$\mathrm{Nu} = \frac{(\xi/8)\mathrm{Re}\,\mathrm{Pr}}{1 + 12.7\sqrt{\frac{\xi}{8}}\,(\mathrm{Pr}^{\frac{2}{3}} - 1)}\, f_1\, f_2\,, \tag{24}$$

where ξ is the tube friction number

$$\xi = (1.8\log\mathrm{Re} - 1.5)^{-2} \tag{25}$$

and factor f_1 considers growing boundary thickness along the tube and f_2 factors in heat flux direction.

$$f_1 = 1 + \left(\frac{d}{l}\right)^{2/3} \tag{26}$$

$$f_2 = \left(\frac{T}{T_{Wall}}\right)^{0.45} \tag{27}$$

VI. ANALYSIS RESULTS

The results of the validation using CFD simulations show the applicability of the analytical formulae for optimization purpose. For single duct geometry with circular and squared cross section the pressure drop and heat transfer was within an accuracy of 2.2 % varying the mean velocity between 5 and 22 m/s.

However, several parallel duct settings are calculated as well with imprinted rotation of the rotor. Thus, the rotor tube inflow shows a deviation from normal direction increasing pressure drop. CFD code (CD-adapco's StarCCM+ Version 8.02.008) with conjugate heat transfer, $k\omega$-turbulenz model and segregated flow was used.

Comparison between CFD results and analytical tool are shown in Fig. 8 and Fig. 9 for 12 random designs ordered with increasing width to height ratio averaged between rotor and stator geometries, each.

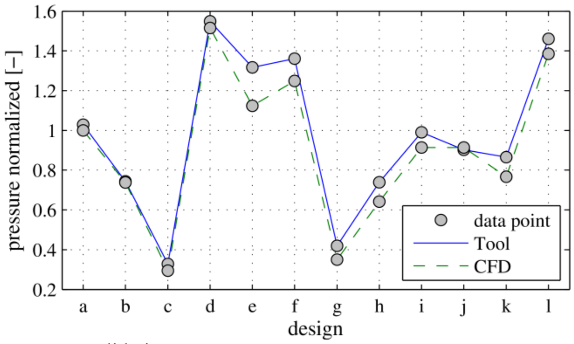

Fig. 8. Pressure validation.

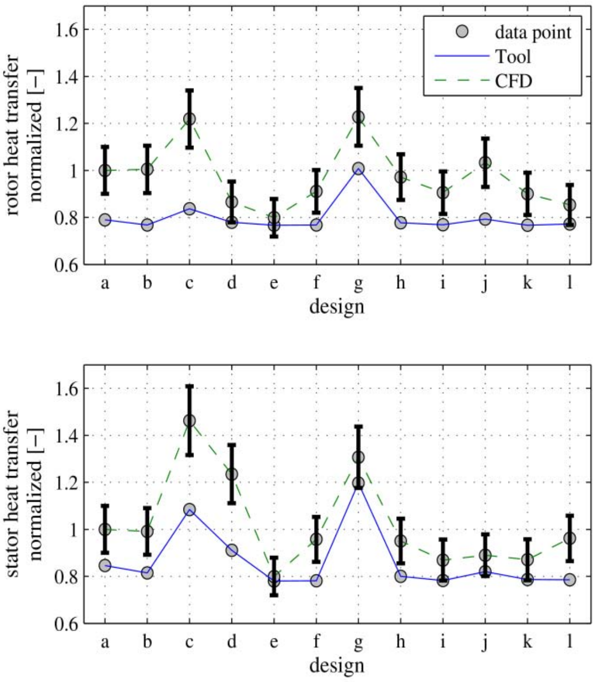

Fig. 9. Heat transfer validation, top rotor, bottom stator.

Results from CFD and analytical tool match very well. The pressure loss is predicted very accurately in most of the cases. Most important for optimization purpose is that the trend is covered correctly which is the case for all designs calculated.

The heat transfer in CFD simulations varies strongly with used turbulence model and mesh settings. Based on this, the error is approximated of about 10 % which is visualized by error bars. Heat transfer is underestimated by the analytical tool but the trend is covered in most cases.

In Fig. 10 the results of the finally performed CFD calculations (for verification purpose of the whole optimization approach) for the initial geometry as well as for the optimized design is depicted. Clear the significantly temperature reduction in the upper motor (optimized cooling design) is visible.

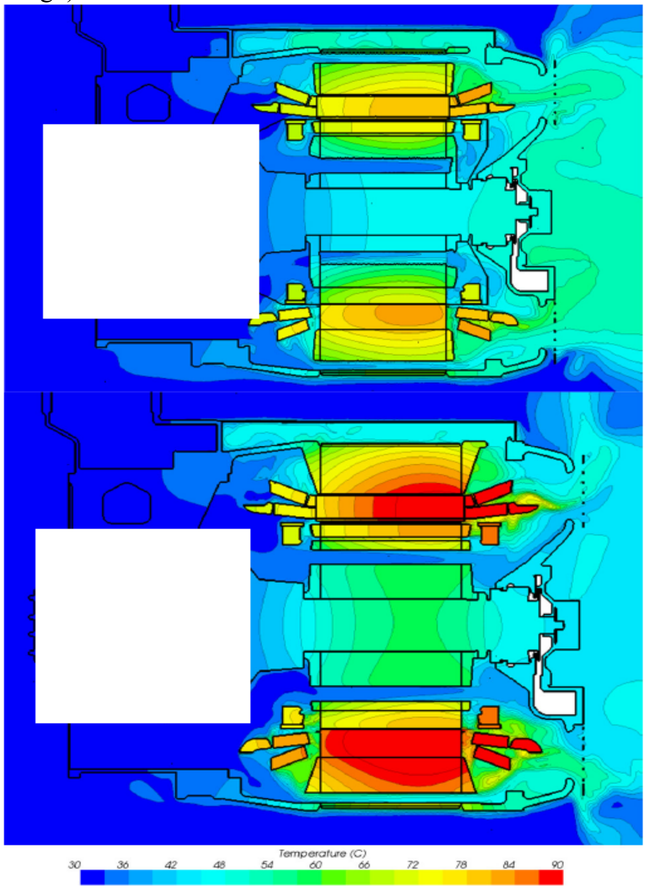

Fig. 10. Temperature distribution calculated by CFD, top: optimized design, bottom: initial design

It can thus be concluded that the proposed cooling optimization approach is working and applicable to achieve a performance improvement of air cooled railway traction drive ac machines.

VII. Conclusion

A new approach for thermal and electromagnetic coupled optimization of induction machines operated in railway traction drives has been presented. The proposed innovative and interdisciplinary optimization method combines very effective tools from electromagnetic finite element calculation and aero-/thermodynamic calculation. The presented results show that analytical equations can be used to model pressure drop, volume flow distribution and heat transfer for optimization purpose. The validation of the model with CFD showed that the pressure drop is predicted very accurately for round geometries whether geometries with large width to height ratio deviate more. However, the trend is covered correctly which is the crucial aspect for optimization. Good coverage of the trend for heat transfer could also be proven because deviation stayed inside the approximated error margin of the CFD. Moreover, the introduced optimization setup shows the implementation of coupled electromagnetic and thermal design evaluation. Finally, an approach is presented to implement an optimization by coupling analytic thermal model, CFD and electromagnetic losses obtained by finite element analysis.

ACKNOWLEDGMENT

The authors want to thank Bombardier Transportation, PPC Drives Development Center1 - Vienna (GSC/NDEW) -electr. calculation group (head Mr. Pfeil, Mr. Moser) and mech. design group (head Mr. Harasleben, Mr. Sieder) for their generous support. Special thanks also goes to Bombardier Transportation - Center of Competence (CoC) Aero- and Thermodynamics in Hennigsdorf (head Mr. Gölz, Mr. Marten, Mr. Mauss) for the great support and feedback. Further the authors want to thank Product Development GSC/PPC Drives (Mr. Bazant) for PDev funding and feedback as well as Mr. Baro (PPC-Drives Global Engineering Head) for the great support.

REFERENCES

[1] J. Pyrhönen, T. Jokinen, and V. Hrabovcová, *Design of Rotating Electrical Machines*. John Wiley & Sons Ltd, 2008.

[2] M. J. Islam, H. V. Khang, A. K. Repo, and A. Arkkio, "Eddy Current Loss and Temperature Rise in the Form-Wound Stator Winding of an Inverter Fed Cage Induction Motor," *IEEE Trans. on Magnetics*, vol. 46, no. 8, Aug. 2010.

[3] H. Gorginpour, H. Oraee, and R. A. McMahon, "Electromagnetic-Thermal Design Optimization of the Brushless Doubly Fed Induction Generator," *IEEE Trans. Industrial Electronics*, vol. 61, no. 4, pp. 1710-1721, 2014.

[4] Z. Yujiao Zhang, R. Jiangjun, H. Tao, Y. Xiaoping, Z. Houquan, and Y. Gao, "Calculation of Temperature Rise in Air-cooled Induction Motors Through 3-D Coupled Electromagnetic Fluid-Dynamical and Thermal Finite-Element Analysis," *IEEE Trans. on Magnetics*, vol. 48, no. 2, pp. 1047-1050, Aug. 2012.

[5] CEDRAT, "User Guide Flux 11," Manual Réf. : K101-111-EN-07/12, 2012.

[6] VDI-Gesellschaft Verfahrenstechnik, *VDI Heat Atlas*, 2nd ed., V. D. Ingenieure, Ed. Berlin: Springer, 2010.

[7] N. Gould, *An Introduction to Angorithms for Countinuous Optimization*. Laboratory, Oxford University Computiong Laboratory and Rutherford Appleton, 2006.

[8] C. R. Reeves and J. E. Rowe, "Genetic Algorithms - Principles and Perspectives: A Guide to GA Theory," *Operation Research/ Computer Science Interfaces Series*, vol. 20, 2003.

[9] J. Schutzhold and W. Hofmann, "Analysis of the temperature dependence of losses in electrical machines," in *Proceedings of Energy Conversion Congress and Exposition (ECCE)*, 2013, pp. 3159-3165.